Molecular Biology of the Cell
Vol. 16, 4096–4107, September 2005

Intermediate Filaments Interact with Dormant Ezrin in Intestinal Epithelial Cells

Flavia A. Wald,* Andrea S. Oriolo,* M. Llanos Casanova,† and Pedro J.I. Salas*

*Department of Cell Biology and Anatomy R-124, University of Miami School of Medicine, Miami, FL 33101; and †Centro de Investigaciones Energéticas, Microambientales y Tecnológicas, University Complutense, E-28040 Madrid, Spain

Submitted March 22, 2005; Accepted June 20, 2005
Monitoring Editor: M. Bishr Omary

Ezrin connects the apical F-actin scaffold to membrane proteins in the apical brush border of intestinal epithelial cells. Yet, the mechanisms that recruit ezrin to the apical domain remain obscure. Using stable CACO-2 transfectants expressing keratin 8 (K8) antisense RNA under a tetracycline-responsive element, we showed that the actin-ezrin scaffold cannot assemble in the absence of intermediate filaments (IFs). Overexpression of ezrin partially rescued this phenotype. Overexpression of K8 in mice also disrupted the assembly of the brush border, but ezrin distributed away from the apical membrane in spots along supernumerary IFs. In cytochalasin D-treated cells ezrin localized to a subapical compartment and coimmunoprecipitated with IFs. Overexpression of ezrin in undifferentiated cells showed a Triton-insoluble ezrin compartment negative for phospho-T567 (dormant) ezrin visualized as spots along IFs. Pulse-chase analysis showed that Triton-insoluble, newly synthesized ezrin transiently coimmunoprecipitates with IFs during the first 30 min of the chase. Dormant, but not active (p-T567), ezrin bound in vitro to isolated denatured keratins in Far-Western analysis and to native IFs in pull-down assays. We conclude that a transient association to IFs is an early step in the polarized assembly of apical ezrin in intestinal epithelial cells.

INTRODUCTION

Ezrin, a member of the ezrin-radixin-moesin (ERM) family, is a conspicuous component of the apical F-actin-based scaffold in simple epithelial cells. It connects NHERF/EBP-50 (which in turn binds important membrane proteins such as CFTR and NHE-3) to F-actin and also enables protein kinase A-mediated regulation of apical channels (Kurashima *et al*., 1999; Louvet-Vallée, 2000; Weinman *et al*., 2000, 2001). Because ezrin is the earliest protein of this complex scaffold to be recruited, it has long been considered as an organizer of the brush border (Bretscher *et al*., 1997). In support of that view, ezrin knockout mice show a distinctive brush-border phenotype with much shorter microvilli that resemble undifferentiated stages (Saotome *et al*., 2004). Furthermore, expression of ezrin in fibroblasts is sufficient to organize microvilli (Shaw *et al*., 1998). After translation, ezrin initially adopts a "dormant" configuration, in which the C- and N-terminal domains bind to each other. On phosphorylation in T567, it changes to an open "active" configuration, freeing the C-terminal domain (C-ERMAND) to bind F-actin and the N-terminal domain (N-ERMAND) to bind NHERF or transmembrane proteins (Bretscher *et al*., 2000). Although the mechanism of activation and assembly of ezrin has been studied in great detail by several groups, the mechanisms that ensure that ezrin assembly occur mostly under the apical membrane of simple epithelial cells remain obscure. Fievet *et al*. (2004) have shown that binding to phosphatidylinositol 4,5-diphosphate (PIP_2) is a prerequisite for activation. However, PIP_2 is not known to be apically polarized in epithelial cells, rather it is basolateral in hepatocytes (Tran *et al*., 1999). A few kinases can phosphorylate T567 (Simons *et al*., 1998), including Rho kinase (Gautreau *et al*., 2000; Yonemura *et al*., 2002), but none of them seem to be apical proteins. In fact, Rho kinase does not affect the brush border, although it does have an effect on endocytosis (Kotani *et al*., 1997). Equally important, Rho activity is basolateral in epithelial cells, regulating basal organization of stress fibers and lateral organization of cell-cell junctions (Takaishi *et al*., 1997; Walsh *et al*., 2001; Van Aelst and Symons, 2002). F-actin is also present at the basolateral domain, in addition to the brush border (Shigeta *et al*., 2003), and yet most newly synthesized ezrin, a cytosolic protein, does not bind basolateral actin that covers more than two-thirds of the inner cortical surface (corresponding to the basolateral surface). Finally, a mechanism that has been postulated to explain the localization of ezrin is the attachment to membrane proteins, including CD44 (Bretscher *et al*., 2000), but CD44 is also basolateral in enterocytes (Gouyer *et al*., 2001). Yet, except for minor basolateral amounts in intestinal crypts (Berryman *et al*., 1993), ezrin is mostly apical. Therefore, why is ezrin not localized mainly to the basolateral domain where one major activation system (Rho), binding sites for the C-ERMAND (F-actin), and for the N-ERMAND (CD44), are present?

Intermediate filaments (IFs) have traditionally been regarded as purely mechanical components of the cytoskeleton. However, recent observations of mistargeting of apical membrane proteins in keratin 8 (K8)-null mice (Ameen *et al*.,

This article was published online ahead of print in *MBC in Press* (http://www.molbiolcell.org/cgi/doi/10.1091/mbc.E05–03–0242) on June 29, 2005.

Address correspondence to: Pedro J.I. Salas (psalas@miami.edu).

Abbreviations used: dox, doxycycline; IF, intermediate filament; K, keratin; PBS, phosphate-buffered saline; PIP_2, phosphatidylinositol 4,5-diphosphate; TX-100, Triton X-100.

2001; Toivola *et al*., 2004) challenge that notion and highlight the existence of poorly understood mechanisms in the development of epithelial polarity that involve IFs. A growing body of evidence suggests that IFs also may determine the subcellular distribution of other proteins and participate in signaling processes, thus exhibiting previously unsuspected scaffolding properties (Coulombe and Omary, 2002; Paramio and Jorcano, 2002). Intermediate filaments are concentrated under the apical domain in a broad range of simple epithelia in culture (Madin-Darby canine kidney cells, Rodriguez *et al*., 1994; MCF-10A and CACO-2 cells, Salas *et al*., 1997) or in vivo (e.g., intestine, Quaroni *et al*., 1993; kidney, Bachman *et al*., 1983; vas deferens, Regadera *et al*., 1997). In the *Caenorhabditis elegans* intestine, the IF protein IFB-2 colocalizes with an ERM ortholog at the apical domain (Van Furden *et al*., 2004). Our laboratory is interested in the hypothesis that IFs may serve as an early scaffold organizing the apical domain in polarized epithelial cells. It was strongly supported by the phenotype of CACO-2 intestinal epithelial cells in tissue culture transiently depleted in IFs (Salas *et al*.,1997) as well as by the phenotype of villus enterocytes in K8-null mice (Ameen *et al*., 2001). In both cases, a specifically apical phenotype comprising diminished or absent apical membrane proteins and disrupted orientation of microtubules (normally apico-basal) was observed. Keratin knockdowns in CACO-2 cells showed shorter and sparser microvilli (Salas *et al*., 1997), but the microvillus phenotype in K8-null mice was only marginal (Ameen *et al*., 2001). The molecular mechanism involved in the disruption of the orientation of microtubules has been pinpointed to a function of IFs attaching microtubule organizing centers (MTOCs) (Salas, 1999; Figueroa *et al*., 2002). The mechanism by which IF down-regulation affected the development of apical microvilli in CACO-2 cells, however, remained obscure. The importance of the apical F-actin-based scaffold in the localization of molecules such as NHERF(EBP-50), CFTR, and NHE-3, among others (Voltz *et al*., 2001), seemed to warrant further analysis of this question. We used keratin knockdowns and keratin overexpression to address this problem and to analyze mechanisms leading to early ezrin localization.

MATERIALS AND METHODS

Antibodies and Plasmids

The antibodies used in this study were as follows: rat monoclonal antibody (mAb) against K8 (TROMA I; Developmental Studies Hybridoma Bank, University of Iowa, Iowa City, IA), anti-K8 (mouse) mAb (Biomeda, Foster City, CA), anti-K7 mAb (RCK105; Accurate Chemical & Scientific, Westbury, NY), anti-K18 mAb (Biomeda), anti-K19 mAb (RCK108; Accurate, Chemical & Scientific), anti-tubulin monoclonal and polyclonal antibodies (Sigma, St. Louis, MO); anti-His-tag (27E8) mAb (Cell Signaling Technology, Beverly, MA), anti-ezrin MAb (Covance, Berkeley, CA), anti-phospho-ezrin (Thr567) polyclonal antibody (Cell Signaling Technology), anti-V5 epitope mAb (Invitrogen, Carlsbad, CA), and nonmuscle actin (C4; MP Biomedicals, Irvine, CA). Affinity-purified secondary antibodies and streptavidin were obtained from Jackson ImmunoResearch Laboratories (West Grove, PA). Fluorescein isothiocyanate (FITC)-phalloidin (Molecular Probes, Eugene, OR) was used at a final concentration of 1 U/ml in addition to the secondary antibodies when necessary. The full-length K8 cDNA was purchased from American Type Culture Collection (Manassas, VA) (#61514) in a pUC18 vector. It was subcloned in the antisense orientation into a pRev-TRE vector (pRevTRE-K8a) (BD Biosciences Clontech, Palo Alto, CA). For transient expression of ezrin, the full-length sense cDNA was cloned into the pcDNA3.1D/V5-His-Topo vector (Invitrogen) in frame with C-terminal V5 and 6xHis tags. The accuracy and orientation of the inserts cloned in each construct were verified by restriction analysis and sequencing.

Cell Lines, Stable and Transient Transfections

PT67 retrovirus-packaging cells (BD Biosciences Clontech) were transfected with either pRev-Tet-ON or pRevTRE-K8a vectors using the Lipofectin transfection system (Invitrogen) and selected in the antibiotic specific for each plasmid (1 mg/ml G418 or 0.4 mg/ml hygromycin, respectively). The supernatants containing the replication-defective retroviruses from each culture were filtered through 0.45-μm SFCA filters and used to infect CACO-2 (human colon carcinoma; American Type Culture Collection) cell monolayers.

CACO-2 cells were kept as described previously (Salas, 1999). For experiments, they were seeded in Transwell inserts (Costar, Cambridge, MA). Some of these cells were first infected with retroviruses carrying the pRev-Tet-ON vectors and selected in 0.15 mg/ml G418. Stable transfectant cloned CACO-2 cells were tested for responsiveness to doxycycline (dox) by transient transfections with pRevTRE-Luc and assayed for dox-induced luciferase expression. Responsive clones (CACO-2Tet-ON) were further infected with retroviruses carrying pRevTRE-K8a and selected for resistance to 0.1 mg/ml hygromycin (CACO-2-K8a cells). For transient transfections, CACO-2 cells were transfected with ExGen 500 (MBI Fermentas, Hanover, MD) according to manufacturer's specifications.

Transgenic Mice and Electron Microscopy (EM)

Transgenic mice overexpressing human K8 (HK8) and their pancreatic phenotype have been described previously (Casanova *et al*., 1995, 1999). In this work, samples from hemizygous HK8-4 (severe phenotype) and HK8-8 (milder phenotype) mice were used for frozen sections and immunofluorescence, or extraction-immunoblot. Tissues for EM were not frozen but directly fixed in 3% glutaraldehyde in 0.2 M phosphate buffer. The extent of mucosal surface affected by a certain phenotype in the intestine was calculated using standard morphometric techniques ($Sv = 4/\pi\, Ba$, where Sv is surface density per unit volume and Ba is section length per unit area; Weibel, 1979).

Cell Extraction, Immunoblot, and Immunofluorescence

Extraction of cytoskeletal proteins from CACO-2 cells and immunoblot were described previously (Salas, 1999). To extract the intestinal mucosa of transgenic or normal mice, ~15-mm-long frozen samples of small intestine were thawed in phosphate-buffered saline (PBS) supplemented with a cocktail of antiproteases [1 mM 4-(2-aminoethyl)benzenesulfonyl fluoride, 0.8 μM aprotinin, 20 μM leupeptin, 40 μM bestatin, 15 μM pepstatin A, 14 μM E-64, final concentrations; P8340, Sigma-Aldrich]. The mucosae were scraped off with the tip of a Pasteur pipette and collected in the same solution. The cells were quickly spun and resuspended in 0.5 ml of PBS supplemented with 1 mM EDTA, 0.5% Triton X-100 (TX-100) and the same cocktail of antiproteases on ice. After 10 min, the suspensions were spun. The pellets were resuspended in PBS, sonicated for 10 s, spun, and resuspended in sample buffer to a final protein concentration of 1 μg/μl. The supernatants were acetone precipitated, dried, and resuspended in sample buffer up to the same protein concentration. Samples of 50 μg of protein were analyzed by SDS-PAGE and blotted. When the blots had to be analyzed with various antibodies, the same nitrocellulose membranes were stripped off and sequentially reprobed with another antibody. Relative band intensities were compared by densitometry.

Immunofluorescence, surface biotinylation, and EM (nanogold) techniques have been described previously (Salas, 1999; Ameen *et al*., 2001). Detergent extractions before fixation for immunofluorescence were performed by incubating the cells in 10 mM sodium phosphate buffer, pH 7.5, 150 mM KCl, 1 mM EGTA, and the same cocktail of antiproteases described above, supplemented with 0.5% TX-100 for 5 min before fixation in formaldehyde. When necessary, DNA was counterstained with DAPI incorporated in the mounting medium. Gold particle counting was performed in nonserial sections from different cells and totaled over the equivalent of 30 μm of section. Confocal microscopy was performed with a Zeiss LSM 510, collecting Z-stacks at 0.4-μm intervals at 0.7 Airy units (normally at 512 $\times$ 512 pixel resolution, except single XY images, acquired at 1024 $\times$ 1024 pixel resolution) without further processing of the images. The images were exported in TIF format using the Zeiss browser, which also was used to convert the stacks to projections when visualization of the whole cell volume was desired.

Metabolic Labeling and Immunoprecipitation

For metabolic labeling, CACO-2 cells 6 d after plating were incubated for 45 min in DMEM without cysteine and methionine and then in the same medium supplemented with 0.58 mCi/ml [^{35}S]methionine/cysteine (Expre; Amersham Biosciences, Piscataway, NJ) for 20 min. The chase was initiated by two rapid washes in regular DMEM. Extraction in TX-100 (PBS supplemented with 1% TX-100, 2 mM EGTA, 1 mM $MgCl_2$, 70 nM phalloidin, and a cocktail of antiproteases), sonication, isolation, and immunoprecipitation of the Triton-insoluble fragments of the cytoskeleton have been described previously (Salas, 1999). Double immunoprecipitation was described previously (Figueroa *et al*., 2002). Briefly, the antibodies were covalently attached to CNBr-activated Sepharose (Amersham Biosciences, Piscataway, NJ). Small multiprotein Triton-insoluble fragments of the cytoskeleton were first immunoprecipitated with Troma I (anti-K8)-Sepharose beads, washed, and eluted in 1% SDS in PBS. The eluate was then diluted 1:5 (vol/vol) in 1% TX-100 (final concentrations: 0.2% SDS, 1% TX-100) in PBS supplemented with 1 mM EGTA. Anti-ezrin antibody coupled to Sepharose was added to this extract for the second immunoprecipitation. For autoradiography, the eluates in sample

buffer were run in SDS-PAGE, blotted onto nitrocellulose, and analyzed with a PhosphorImager.

Keratin and Ezrin Purification and Phosphorylation: Blot Overlays and Pull-Downs

Keratins from CACO-2 cells were purified by cycles of solubilization in urea and repolymerization in saline (Steinert *et al*., 1982). Full-length ezrin cDNA (obtained from Open Biosystems, Huntsville, AL) was cloned into the pACHLT-C vector (BD Biosciences PharMingen, San Diego, CA) with a C-terminal 6xHis tag and used to cotransfect Sf9 insect cells with Baculogold DNA (BD Biosciences PharMingen). The recombinant baculovirus produced was used to infect Sf9 monolayers at ~10 MOI. The cells were harvested in radioimmunoprecipitation assay buffer (150 mM NaCl, 50 mM Tris-HCl, 1% NP-40, 0.5% sodium deoxycholate, and 0.1% SDS, pH 8.0) supplemented with antiprotease and antiphosphatase cocktails (Sigma-Aldrich) 2 d later. The extracts were purified on Ni^{2+} columns (ProBond resin; Invitrogen) using the nondenaturing protocol provided by the manufacturer. The resin was extensively washed in 50 mM imidazole and then eluted in 350 mM imidazole. This eluate was desalted/concentrated by ultrafiltration and showed a single band visible by Coomassie Blue staining that reacted positively in immunoblot with anti-ezrin and anti-His tag antibodies. After concentration by ultrafiltration, ezrin was resuspended in protein kinase C (PKC)θ buffer (20 mM MOPS, pH 7.2, 25 mM β-glycerophosphate, 1 mM sodium orthovanadate, 1 mM dithiothreitol, 1 mM $CaCl_2$, and supplier-provided lipid activator) and phosphorylated (or not, control) with 4 U/ml recombinant active PKCθ (Upstate Biotechnology, Lake Placid, NY) in the presence of 1 mM ATP. Ezrin phosphorylation was tested with anti-T567 ezrin antibody by immunoblot and by assaying F-actin binding activity in pull-down assay on phalloidin-stabilized F-actin (Cytoskeleton, Denver, CO) covalently attached to CNBr-activated Sepharose beads. In pull-down assays, samples of input (typically 10%), eluates from the beads after extensive washes, and proteins in the supernatant after pull-down (concentrated by StrataClean resin beads; Stratagene, La Jolla, CA) were analyzed by immunoblot.

For blot overlays, purified keratins or other (control) proteins (~10 μg/lane) were separated by standard SDS-PAGE and blotted onto nitrocellulose. Nitrocellulose strips were washed in PBS, quenched with 1% casein, 0.1% NP-40 in PBS for 1 h, and incubated with the appropriate ligands for 2 h. Then, the strips were washed extensively with 0.1% NP-40 in PBS and incubated with the appropriate antibodies according to a standard immunoblot procedure followed by chemiluminescence. For ezrin pull-down with IFs, purified native keratins polymerized in filaments were obtained as described above (Steinert *et al*., 1982), finely homogenated by extensive sonication (Rodriguez *et al*., 1994), and covalently attached to CNBr-activated Sepharose beads.

RESULTS

Intermediate Filaments Are Necessary for the Formation of the Apical Ezrin Scaffold in CACO-2 Cells

To mimic in tissue culture previous findings in K8-null mice (Ameen *et al*., 2001), we first sought a stable IFs knockdown in CACO-2 cells lasting until the cells were fully polarized. To this end, we obtained stable transfectants of CACO-2 cells expressing an antisense K8 RNA under a Tet-responsive element (CACO-2-K8a). This keratin was chosen because it was found to be the only type II keratin present in CACO-2 cells at advanced stages of polarization and differentiation (Salas *et al*., 1997). Therefore, because keratins are obligate heterodimers requiring one type II partner, the down-regulation of K8 has a more complete effect on the overall amount of IFs than the manipulation of either type I keratin (K18 or K19). In CACO-2-K8a cells, the amount of K8 in the absence of dox did not change significantly between 5 d (before polarization) or 14 d (fully polarized stage) after seeding the cells (Figure 1A). Monolayers continuously incubated in dox, on the other hand, showed a reduction in K8 (Figure 1A). A modest amount of K7 (another type II keratin that could replace K8) was found in the 5-d stage (mimicking K7 expression in less differentiated crypt enterocytes; Baribault *et al*., 1994), but none was observed in the 14-d stage, just like in fully differentiated enterocytes (Ameen *et al*., 2001). More importantly, in monolayers continuously cultured in dox, K7 was not up-regulated (Figure 1A).

The expression of K8 and F-actin was analyzed by confocal microscopy in CACO-2-K8a cells cultured for 14 d in the presence (+) or absence (−) of dox. To ensure that the images show the entire volume of the cells, projections of the Z-axis stack of confocal images are shown in Figure 1, B–D. When the K8 antisense RNA was induced, lower levels of K8 were observed (Figure 1B, dox+). The effect, however, was variable in different cells. In a subpopulation of cells (~10%) there was no effect. In a large proportion of the cells (70–80%), there were less IFs than in the control (dox−, the images were acquired at exactly the same gain); and, finally, in some cells the lack of IFs was nearly total (Figure 1B, +, red). Fluorescent-phalloidin in those K8-depleted cells showed a substantial lack in the apical actin organization as well (Figure 1B, +, green). In the same experiment, the distribution of ezrin was similar to that of F-actin in the apical domain in control cells (Figure 1C, dox−). In dox+, in contrast, CACO-2-K8a cells showing the greatest K8 down-regulation, also lacked ezrin (Figure 1C). At this point, however, it was unclear whether ezrin was reporting on the lack of microvilli or, as one of the organizers of microvilli, the lack of apical ezrin was a causal factor for the lack of apical F-actin. To answer this question, CACO-2-K8a cells were continuously kept in dox and transfected with full-length human ezrin tagged with a C-terminal V5 epitope on day 4. The cells were fixed 6 d later (i.e., 10 d after seeding) and stained as described above with the addition of the V5 epitope that was localized with CY5-coupled secondary antibody in the far-red (blue) channel. Cells expressing high and low levels of K8 were equally transfected, but we focused our analysis on those cells deeply down-regulated in K8 that, in addition, were overexpressing V5-ezrin (Figure 1D). The apical F-actin images of these cells cannot be compared with the more differentiated cells shown in Figure 1, B and C. However, apical F-actin in cells depleted in IF and overexpressing ezrin was more developed than in nontransfected neighboring cells also expressing very low levels of K8 (Figure 1D, arrows). This result suggested that ezrin overexpression rescued the F-actin phenotype to some extent and that the low levels of apical ezrin in K8 knock-down cells play a role in the absence of apical F-actin. Comparing apical F-actin images in the transfected cells with cells with normal or nearly normal amounts of IFs (e.g., Figure 1D, two cells at the bottom of the image), however, indicated that the rescue was partial.

Finally, we wanted to analyze whether ezrin was stable after its assembly in the apical scaffold. To that end, CACO-2-K8a cells were incubated in the absence of dox for 12 d and assayed for K8 (Figure 1E, red) and ezrin (Figure 1E, green), with results identical to those in Figure 1C. Parallel monolayers were switched to dox for 2 d before fixation. Although the decrease in K8 was not perfectly synchronized, by the second day the proportion of cells with low levels of K8 (Figure 1E, red, right-hand side) was similar to those of monolayers continuously kept in dox (Figure 1C). However, there was a substantial proportion of cells with low levels of K8 that still showed apical ezrin (Figure 1E, arrows; also XZ confocal sections). The proportions of cells with low levels of K8 and still showing ezrin were as follows: day 1 (after switch to dox), 64%; day 2, 57%; day 4, 15%; and day 6, 6% (images shown for day 2 only; Figure 1E). These data suggested that once ezrin is assembled at the cell surface, it becomes stable and less dependent on the integrity of IFs.

Overexpression of K8 Results in Ezrin Redistribution to a Subapical Compartment in Transgenic Mice Enterocytes

Although the effects of K8 knockdown shown above could be explained in several possible ways, evidence from other laboratories and our own work point at possible scaffolding

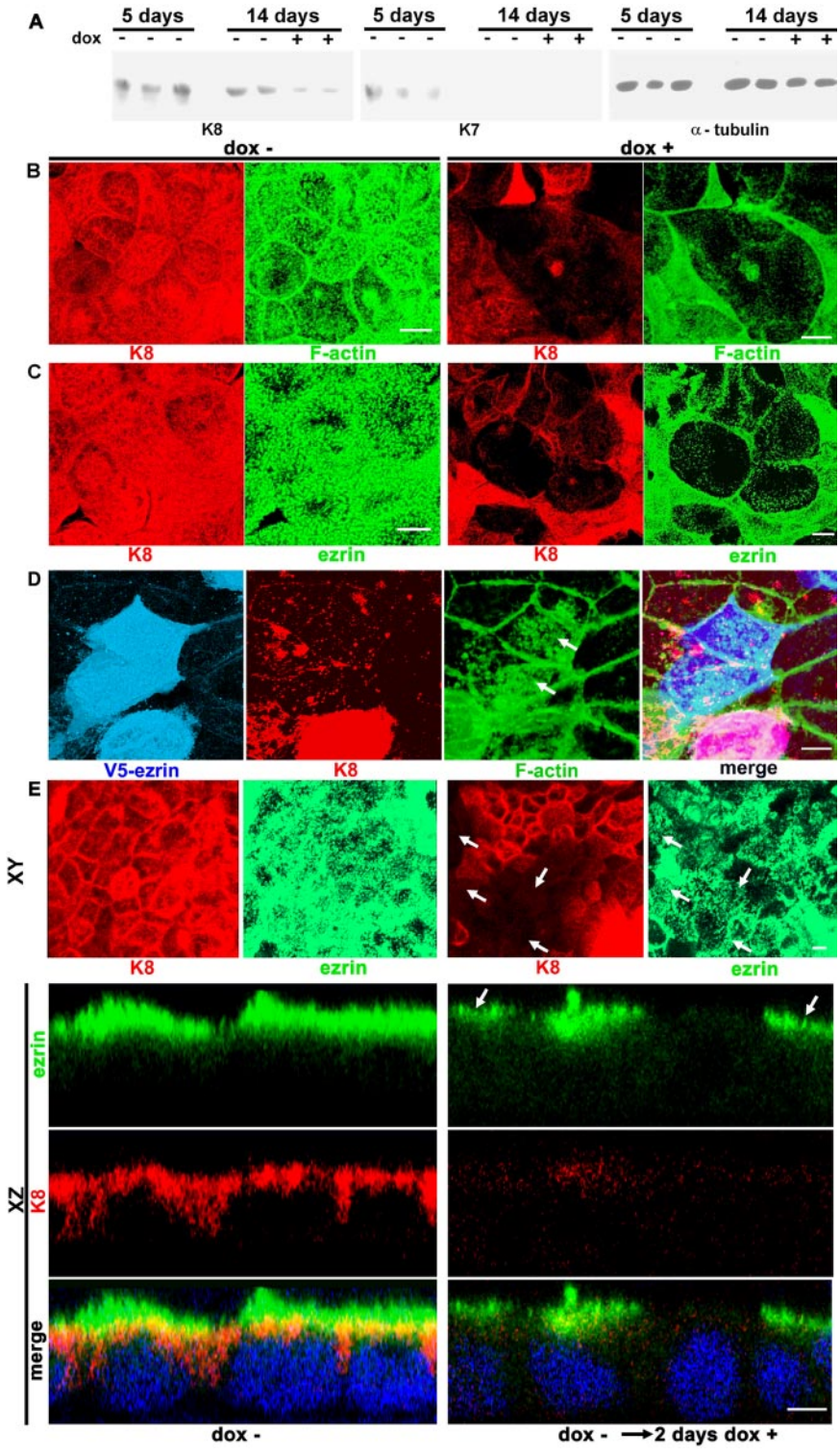

Figure 1. Intermediate filaments are necessary for the organization of the F-actin submembrane cytoskeleton. (A) Stable CACO-2 cell transfectants expressing a K8 antisense RNA under a Tet-ON tetracycline-inducible promoter (CACO-2-K8a) were kept continuously in the absence (−) or presence (+) of 1μg/ml dox and extracted at 5 or 14 d after plating. The extracts from triplicate (5 d −) or duplicate (14 d − or +) monolayers were analyzed by immunoblot, on the same membrane, consecutively with anti-K8, anti-K7, and anti-tubulin antibodies. (B) The same CACO-2-K8a cells were kept for 14 d in the presence (dox+) or absence (dox−) of 1 μg/ml dox, fixed in 3% formaldehyde, and processed for indirect immunofluorescence for K8 (red channel) and FITC-phalloidin (green channel). (C) An identical experiment as in B, but the cells were processed for indirect immunofluorescence with anti-ezrin mAb (green channel). (D) In a similar experiment, all the cells were continuously incubated in dox. Four days after seeding, the cells were transfected with V5-tagged ezrin and fixed 6 d later. The V5 epitope was visualized with Cy5-labeled antibody in the far-red (blue) channel along with K8 (red) and F-actin (green). B–D are projections of all the confocal sections in a Z-stack comprising the entire volume of the monolayer. The gains in B and C for each separate channel were the same for + and −. Because of the difference in fluorescence intensities, some saturation was allowed in the controls (−) to show detail of the low-expression cells in +dox. Likewise, the gain in D was set to show expression levels in cells down-regulated in K8, and therefore, normally expressing cells seem saturated. (E) Top, XY projections of CACO-2-K8a cells cultured for 12 d (dox−) or switched to dox for the last 2 d before fixation (dox− → dox+). Bottom three rows, XZ sections of the same monolayers. In all panels, the labels were as follows: green, ezrin, and red, K8. DAPI stain for DNA (blue) was added for the merge of the XZ images only. The arrows point at K8 negative cells that still show apical ezrin. Bars, 5 μm.

properties of IFs. To explore the possibility that the defect in F-actin and ezrin observed above may be due to IF-dependent localization of ezrin and F-actin, we analyzed the phenotype of transgenic mice that overexpress a tandem of at least 17 copies of the human K8 (hK8) gene under its natural promoter (Casanova *et al*., 1995, 1999). The rationale for this approach is that if IFs serve as a scaffold for ezrin or F-actin, overexpression and mislocalization of IFs is expected to cause a redistribution of these proteins. In this work, we analyzed tissues from hemizygous HK8-4 animals that display a severe phenotype (the homozygous animals die within a few days after birth) and from HK8-8 mice that display a milder phenotype. To assess the overexpression of K8 and its incorporation into IFs, the intestinal mucosae of HK8-8 (Figure 2, two animals, lanes 3 and 4), and HK8-4 animals (Figure 2, two animals, lanes 5 and 6) were com-

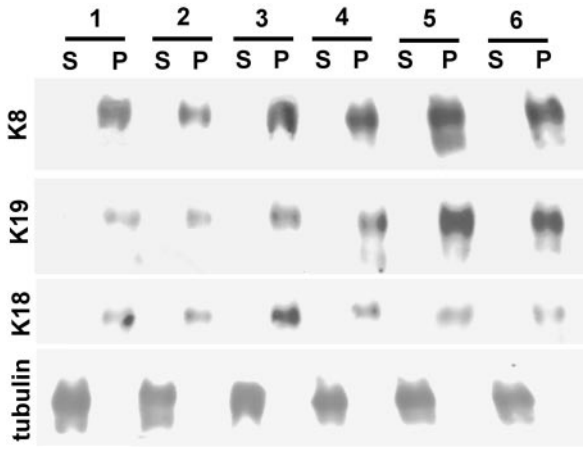

Figure 2. Overexpression of keratins in transgenic mice. The mucosae of small intestine segments from two HK8-8 animals (3 and 4), two HK8-4 animals (5 and 6) and two normal littermates (1 and 2) were extracted in TX-100 in the cold and centrifuged. The pellets (P) and the acetone precipitates of the supernatants (S) (50 μg of total protein/lane) were run in SDS-PAGE and blotted. The same blots were consecutively probed with anti-K8, anti-K19, anti-K18, and anti-tubulin (as a load control) antibodies by chemiluminescence.

pared with those of normal littermates (Figure 2, two animals, lanes 1 and 2). In each case, TX-100-insoluble pellets (cytoskeletal preparation; Figure 2, P) were compared by immunoblotting with the acetone precipitates from the corresponding supernatants (Figure 2, S) normalized by total protein. On average, K8 increased 1.7-fold in the HK8-8 mucosae compared with the samples from normal epithelia and 2.8-fold in the HK8-4 animals (Figure 2). We failed to find any K8 in the supernatants, suggesting that soluble K8 monomers were not abundant in these cells. The same nitrocellulose membranes were sequentially reprobed with anti-K19 and anti-K18 antibodies. K19 was up-regulated in all cases and K18 seemed up-regulated in some animals as well (Figure 2). These samples had been frozen and were extracted in the cold without any measures being taken to preserve microtubules, so tubulin was found in the supernatants and used as load control. These results indicate that overexpressed K8 is incorporated into IFs (in K8-K18 and K8-K19 dimers) in HK8-4 and HK8-8 transgenic mice in a way that correlates with the penetrance of the phenotype.

The structure of the brush border and the distribution of IFs, F-actin, and ezrin were analyzed in sections of villus enterocytes from HK8-8 and HK8-4 animals. The phenotypes were similar, but the extent of the lesions was always larger in HK8-4 cells. The apical brush border visualized with FITC-phalloidin in control animals disappeared in 40–98% of the apical surface in HK8-4 animals (Figure 3A; n = 4) and in 10–26% of the apical surface in HK8-8 animals (n = 4; our unpublished data). The same result was visualized in transmission EM as a substantial decrease in the number and length of microvilli (Figure 3B), a phenotype that resembles that of ezrin knockout mice (Saotome *et al*., 2004). An extensive increase in the number of cytoplasmic IFs was observed in frozen sections of HK8-4 (Figure 3D, red) and HK8-8 enterocytes (our unpublished data). In both cases, the apical submembrane layer of apical IFs was always more prominent than in control animals (Figure 3C, red), and keratin increased also to various extents in the rest of the cytoplasm. In normal cells, ezrin was mainly localized to the apical domain at or above the level of keratins, as expected from microvilli (Figure 3C, green), with only minor amounts in the basal domain, compatible with previous reports (Poullet *et al*., 2001). In HK8-4 enterocytes, however, it largely distributed throughout the cytoplasm (Figure 3D, arrows). In these cells, there was less apical ezrin compared with controls, and a substantial amount of ezrin signal was observed as coarse (0.1–0.5 μm in diameter) spots localized alongside keratin signal (Figure 3E). It is worth noticing that this abnormal localization of ezrin in the cytoplasm in HK8 enterocytes overexpressing keratins did not equate with the distribution of F-actin that was greatly decreased in the apical domain and absent from the cytoplasm, except for the basolateral cortical distribution (Figure 3A). It is also important to mention that kidney and liver epithelia from HK8-4 and HK8-8 animals were analyzed by phalloidin fluorescence and EM, and they did not show a decrease in apical microvilli (our unpublished data).

Triton X-100-insoluble Ezrin Occurs in an Apical Submembrane Keratin Compartment

Because ezrin is known to be attached to F-actin (via the C-terminal domain) and to membrane proteins (via the N-terminal domain), we explored the alternate hypothesis, namely, that the redistribution of ezrin in HK8 animals may be due to the depletion of apical F-actin (Figure 3A). To test this idea, we used an extensive cytochalasin D treatment in CACO-2 cells. We colocalized in XZ confocal sections ezrin (blue), F-actin (FITC-phalloidin, green), and the apical membrane itself by surface biotin derivatization with a membrane-impermeant biotinylation agent (red) in CACO-2 cells (Figure 4A). In control cells, all three labels were observed at the apical domain with extensive colocalization of ezrin and biotin signals (Figure 4A, merge, white signal). After a 5-h incubation in cytochalasin D, F-actin was largely discontinuous (Figure 4A, right-hand side, green). Yet, ezrin was still localized to the apical domain (Figure 4A, blue) in a continuous layer, suggesting that the change in localization observed in the keratin overexpression scenario is not a consequence of the disruption of apical F-actin. However, no clear colocalization of ezrin with the membrane biotin signal in the Z-axis was observed in cytochalasin-treated cells. If the remaining ezrin was localized to the apical membrane by its N-terminal domain, it would have been expected to be only a few nanometers away from the biotin signal on the outside of the membrane. Instead, in many confocal stacks, ezrin signal was observed in the confocal section immediately below that of the membrane signal. Because this observation is difficult to document, it is within the limit of resolution of the confocal microscope in the Z-axis, and therefore could be explained by simple refraction artifacts, we decided to repeat the same experiment using electron microscopy. In control cells, most of the ezrin signal, identified by immunogold, was located in the microvilli (Figure 4B, 1); however, 29% of the gold particles were found within a narrow area of the apical cytoplasm up to 1 μm below the apical membrane (blue bars). In cells treated with cytochalasin D, as expected, most microvilli disappeared (Figure 4B, 2). However, 71% of the gold particles labeled ezrin below the membrane (Figure 4B, red bars). In fact, the average distance between the gold particles and the membrane, in cytochalasin-treated cells, was 0.4 $\pm$ 0.2 μm from the apical membrane, that is, almost 100 ezrin Stokes radii from the membrane. Therefore, the continuity of the apical ezrin layer observed by confocal microscopy in cytochalasin-treated cells (Figure 4A, blue) cannot be explained either by binding to the membrane or to F-actin. Ezrin must have an additional novel binding capability that keeps it in the general vicinity

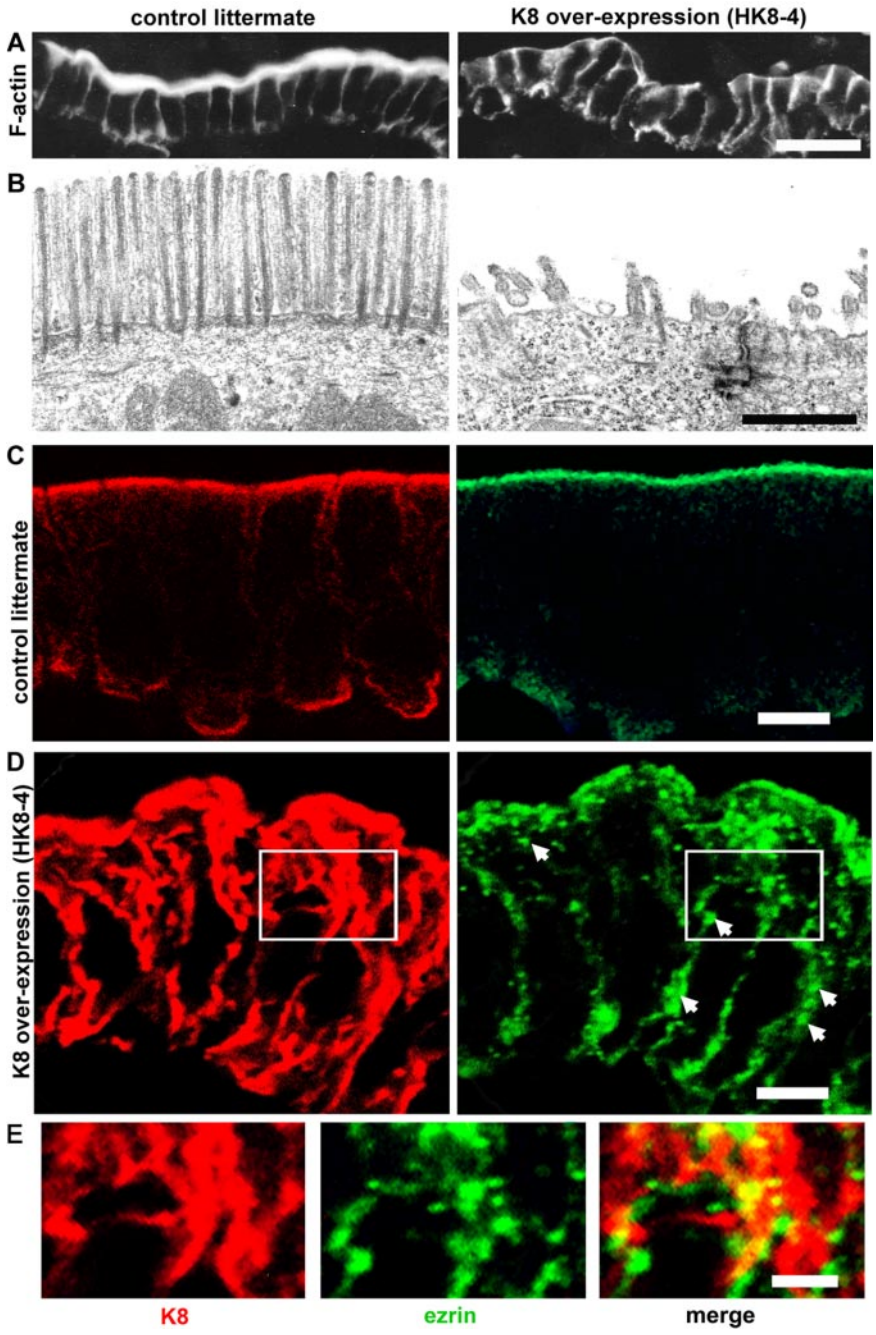

Figure 3. Overexpression of K8 and intermediate filaments prevents assembly of the brush border in transgenic mice. (A) Frozen sections of HK8-4 transgenic mice (K8 overexpression) small intestine or from control littermates were probed with FITC-phalloidin (F-actin). (B) Transmission electron-microscopy of the same samples as in A. (C) Confocal microscopy of frozen sections from control littermate animals using anti-K8 (red channel) or anti-ezrin antibodies (green channel). (D) Sections from an HK8-4 animal were processed as in C. Arrows point at cytoplasmic ezrin label located throughout the cytoplasm. E shows an enlargement of the areas boxed in D. Bars, 20 μm (A), 1 μm; (B), 10 μm (C and D), and 5 μm (E).

of the apical membrane in the absence of a continuous F-actin layer.

Because this distribution of ezrin in cytochalasin D-treated cells is coincidental with the localization of apical IFs, and bearing in mind our hypothesis of a scaffolding function of IFs, we repeated the same experiments, but the TX-100-insoluble cytoskeleton was subjected to immunoprecipitation with an antibody against K8. To this end, we immunoprecipitated intermediate filaments under nondenaturing conditions in small fragments separated by sucrose gradients (Rodriguez *et al*., 1994; Salas, 1999; Figueroa *et al*., 2002). Although the yield is poor and the proportion of fragments useful for immunoprecipitation is relatively small (top half of the gradient), we demonstrated that these fragments represent a random sampling of the cytoskeletal preparation (Salas, 1999). Aliquots of the inputs were blotted as well. In untreated cells, a modest amount of ezrin coimmunoprecipitated with K8 (Figure 4C, ezrin blot, − +). However, treatment with cytochalasin D resulted in a ninefold increase in the ezrin coimmunoprecipitating with K8 (Figure 4C, ezrin blot, ++), supporting the notion that attachment to IFs is sufficient to maintain the apical localization of ezrin in cytochalasin D-treated cells. This increase in ezrin coimmunoprecipitating with K8 occurred despite a decrease in the total ezrin in the input from cytochalasin treatment. Interestingly, although actin was present in the input, we failed to find it coimmunoprecipitating with K8 (Figure 4C, actin blot). This result does not rule out the presence of trace amounts of actin below the threshold of detection of the method. However, the enrichment in ezrin and keratin (Figure 4C, K8

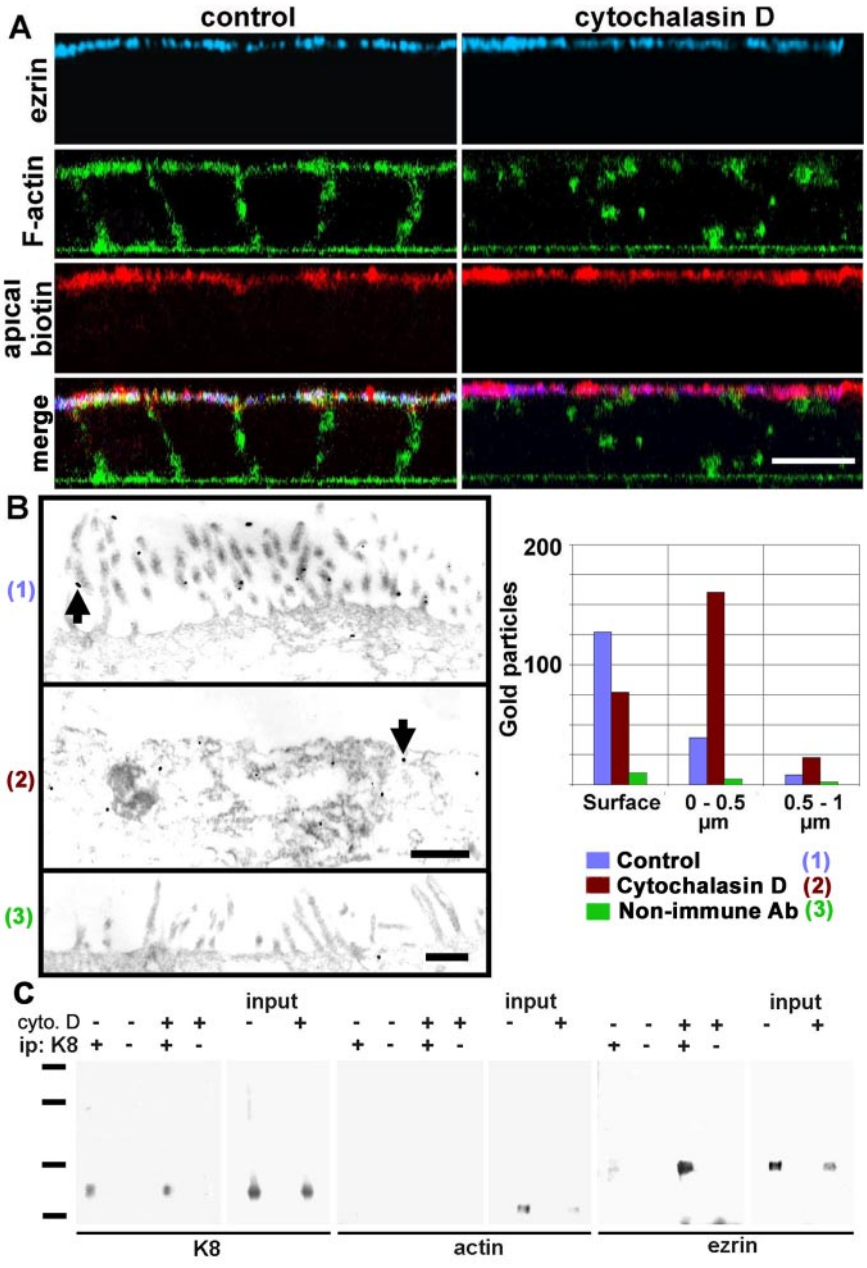

Figure 4. Apical localization of ezrin is independent of F-actin and the membrane in cells treated with cytochalasin D. (A) CACO-2 cells were treated with or without (control) 2 μM cytochalasin D for 5 h, surface-biotinylated on the apical side, and fixed in formaldehyde. The cells were processed with anti-ezrin antibody (blue), fluorescent phalloidin (green, F-actin), and fluorescent streptavidin (red, apical biotin) and analyzed by confocal microscopy. The images are presented as XZ sections with the apical side up. (B) In similar experiments, the cells also were treated with cytochalasin D (2), processed with anti-ezrin antibody (1 and 2), or with nonimmune antibody (3) and processed with nanogold particles for EM. Arrows show examples of gold particles. Total gold particle counting over 30 μm of section in photographs from nonserial sections is shown for the surface (particles in contact with the plasma membrane including microvilli), a band of apical cytoplasm between 0 and 0.5 μm, or between 0.5 and 1 μm below the apical plasma membrane. Bars, 10 μm (A), 0.7 μm (B). (C) CACO-2 cells were incubated with (+) or without (−) cytochalasin D (cyto.D) as described above and extracted in TX-100 in the presence of antiproteases. The Triton-insoluble pellets from 1.5×10^7 cells were then fractionated by sonication, and the smallest multiprotein complexes were immunoprecipitated with anti-K8 antibody (ip +) or nonimmune IgG (ip −) and analyzed by immunoblot with anti-K8, anti-actin, or anti-ezrin antibodies. Standards, 201, 127, 86, and 37 kDa.

blot) over actin in this immunoprecipitation dispels the possibility that keratin and ezrin coimmunoprecipitation is mediated by actin. The question of whether this interaction is direct or indirect (mediated by other proteins) is addressed in the last section of Results. Along with the distribution of gold particles in Figure 4B, these results indicate that there is a small physiological compartment of TX-100-insoluble endogenous ezrin bound to IFs in steady-state conditions.

A Submembrane Compartment of Triton-insoluble Dormant Ezrin Is Present in Nondifferentiated Cells

The submembrane cytoskeleton of IFs and F-actin was analyzed in CACO-2 cells in the stages before the development of apical membrane polarity, that usually starts after 5 d in culture. Using three-dimensional XZ reconstructions of confocal stacks, a substantial increase in apical F-actin is observed on day 5, coincident with the onset of microvillar organization (Pinto *et al.*, 1983) as opposed to basal stress fibers in 3-d cells (Figure 5A, green, arrows). The IFs, on the other hand, were predominantly apical (or apico-lateral) on day 3, well before the organization of the brush border starts (Figure 5A, red), except in very flat cells in which IFs were still distributed throughout the cytoplasm (our unpublished data). In other words, the apical polarization of IFs precedes that of F-actin. If F-actin guided the localization of ezrin, one would expect ezrin to be basal before the 5-d stage. Therefore, the 3-d stage represents an ideal benchmark to assay the driving force that determines the distribution of ezrin before it reaches the membrane. The only caveat is that little endogenous ezrin is expressed at this stage. To overcome this problem, we transfected CACO-2 cells with V5-tagged ezrin at days 2 or 5 after plating. Then, after 24 h, cells representing the undifferentiated stage (Figure 5, B–D, 3 d) or the onset of actin polarization described above (Figure 5,

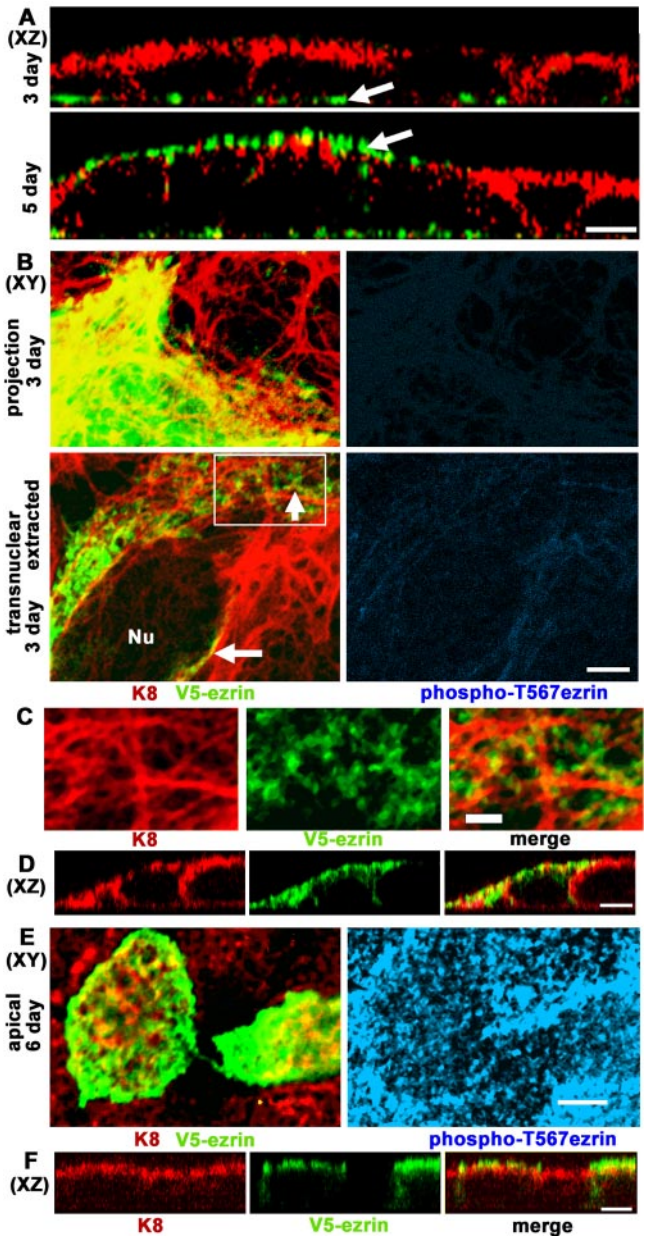

Figure 5. Triton X-100-insoluble dormant ezrin localizes below the membrane alongside intermediate filaments in undifferentiated cells before the onset of brush border formation. (A) CACO-2 cell monolayers at 3 or 5 d after plating were processed for F-actin fluorescence (phalloidin, green channel) and indirect immunofluorescence for K8 (red channel). The images represent XZ reconstructions of confocal optical section stacks (apical side up). (B–F) CACO-2 cells were transiently transfected with V5-tagged (C-terminal) h-ezrin 1 d before fixation. (B–D) CACO-2 cells were fixed 3 d after plating. (B) Projections of the entire confocal stack from nonextracted cells showed abundant V5-ezrin in the cytoplasm of transfected cells (top). Single XY confocal sections (bottom) at a transnuclear plane (Nu, nucleus) of TX-100-extracted cells showed V5-ezrin (anti-V5 antibody, green) and K8 (red) below the apical membrane (arrows). The right hand side panels show the blue channel for the anti-pT567 ezrin antibody at a similar gain as in E, right-hand side panel. (C) An enlargement of the area boxed in B showed coalignment of the TX-100-insoluble ezrin spots (green) and IF bundles (red). (D) XZ sections of 3-d TX-100-extracted cells showing K8 (red) and V5-ezrin (green). (E) The same experiment was performed in cells 6 d after plating and shows single confocal XY images through the apical domain. (F) XZ sections were obtained through the same fields. Anti-pT567 ezrin signal (blue) was positive only in cells after day 5. Bars, 10 μm (A), 5 μm (B, D–F), and 2 μm (C) (notice that 3-d cells are more spread than 6-d cells).

E and F, 6 d) were fixed and analyzed by immunofluorescence. All transfected cells showed some degree of V5 epitope signal evenly distributed throughout the cytoplasm (Figure 5B, top panels show projections of the entire confocal stack), but when the cells were extracted in TX-100 for 5 min before fixation, Triton-insoluble ezrin signal spots were found along IF bundles in transnuclear single confocal planes (Figure 5B, arrows, and C, enlargement of boxed area). The same fields showed no reactivity for anti-phosphoT567 ezrin (Figure 5B, blue), suggesting that both soluble and Triton-insoluble V5-ezrin was dormant in 3-d cells. In XZ confocal sections, the TX-100-extracted cells showed ezrin codistributing with apical and lateral IFs, or immediately below them (Figure 5D). When the same experiment was performed on 6-d cells, the Triton-insoluble ezrin occurred in apical confocal planes and microvilli (Figure 5E, green), and the microvilli of both transfected and nontransfected cells were positive for phospho-T567 ezrin (Figure 5E, blue). The presence of V5-ezrin in the apical domain, mostly above the IF layer was confirmed in XZ sections of the same fields (Figure 5F). In other words, overexpressed Triton-insoluble ezrin accumulated in a subapical IF scaffold in undifferentiated cells in the dormant form, but it readily incorporated into the apical scaffold and microvilli after the onset of brush-border assembly.

Transient Association of Ezrin with IFs in Differentiating Cells

The results from knockdown experiments (Figure 1) and overexpression (Figure 3) suggest that IFs play an important role in the distribution of ezrin. However, ezrin is physiologically located in microvilli where IFs are absent and the size of the submembrane pool in normal differentiated cells is very modest as determined before by morphological and biochemical techniques (Figure 4). To explain this paradox, we hypothesized that in differentiated cells with an established brush border, the attachment of ezrin to IFs may be transient. To test this hypothesis, we conducted pulse-chase experiments on confluent CACO-2 cells. Six days after seeding, the cells were pulsed with [^{35}S]methionine-cysteine and then chased for various times (10–120 min). At each time, the Triton-insoluble pellet was solubilized and immunoprecipitated with anti-ezrin antibody. PhosphorImager images showed 80- and 64-kDa bands (Figure 6, arrows). We do not have an explanation for this double-band pattern, as opposed to the typical 80-kDa ezrin mobility in immunoblots. It is worth to note, however, that the mass of ezrin predicted by its sequence is 64 kDa and that Louvet-Vallée et al. (2001) found that ezrin can be *O*-glycosylated. More importantly, ezrin was incorporated into the total cytoskeleton (containing both keratins and actin; Figure 4C) in a bimodal manner with a peak at early times, a decrease at 30–40 min, and a second stable incorporation after 1 h (Figure 6A). To dissect what part of these complex kinetics corresponds to incorporation onto intermediate filaments, the TX-100-insoluble cytoskeleton from labeled cells also was homogenated by extensive sonication. The small multiprotein fragments useful for immunoprecipitation were recovered from the top of a sucrose gradient as in Figure 4C, and immunoprecipitated with anti-K8 antibody first under nondenaturing conditions.

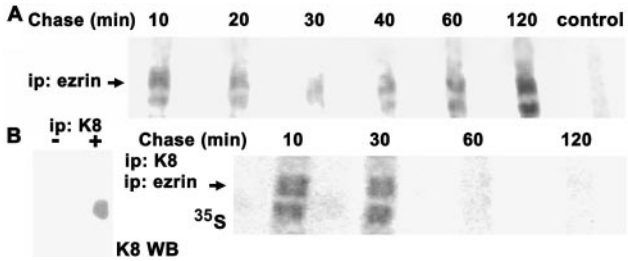

Figure 6. Newly synthesized ezrin transiently attaches to intermediate filaments. (A) Six-day CACO-2 monolayers were pulsed with [^{35}S]methionine-cysteine for 20 min and chased for various times (10–120 min). The Triton-insoluble cytoskeleton was separated by centrifugation and solubilized in 1% SDS. Then, the supernatant was diluted to 0.2% SDS, 1% TX-100 immunoprecipitated with anti-ezrin antibody, or a pool of aliquots (1/6 of each sample) of all the other samples was immunoprecipitated with nonimmune IgG (control), and analyzed by SDS-PAGE and PhosphorImager. (B) The Triton-insoluble cytoskeleton from cells pulsed and chased as described in A, homogenated by sonication, and the small multiprotein fragments were immunoprecipitated with anti-K8 (TROMA I) antibody first. This first immunoprecipitation was controlled with parallel nonlabeled cytoskeletal fragments assaying the eluates by immunoblot with an anti-K8 mouse mAb (left, K8 WB). Then, the material was eluted in 1% SDS, diluted to 0.2% SDS, 1% TX-100 and immunoprecipitated again with anti-ezrin antibody. Finally, the second eluate was separated by SDS-PAGE and analyzed by PhosphorImager (right-hand side panel). The arrows point at the 80-kDa band in a typical PhosphorImager image of four experiments. The apparent mass of the lower band is 64 kDa.

Positive controls for this first immunoprecipitation were performed in parallel nonlabeled cytoskeletal fragments (Figure 6B, left). To assess ezrin among a number of other labeled proteins (including newly synthesized keratins), the eluates in SDS from the first immunoprecipitation, were diluted in an excess of TX-100 and reimmunoprecipitated with an anti-ezrin antibody. The eluates of this second immunoprecipitation were analyzed by SDS-PAGE and PhosphorImager (Figure 6B). Despite the total amount of counts in all inputs was the same, the IF-associated ezrin was conspicuous at 10 and 30 min of the chase, but it almost disappeared at 60 and 120 min. Bearing in mind that immunoprecipitation of TX-100-insoluble fragments of the cytoskeleton with anti-K8 antibody results in a preparation highly depleted in actin (Figure 4C), this result suggests that, in differentiating cells, newly synthesized ezrin associates with IFs. Ezrin then remains attached to IFs for <1 h, and only marginal amounts may continue to be associated for longer times.

Dormant (but Not Active) Ezrin Binds Directly to Keratins In Vitro

Two questions arose from the previous results: 1) Is ezrin attaching directly or indirectly to keratins? and 2) Because most of the attachment seems to occur very early after the synthesis of ezrin, does it occur before ezrin is activated (dormant form) or after phosphorylation in T567 (active form)? To answer these questions, we cloned full-length ezrin in frame with a C-terminal 6xHis tag into a baculovirus transfer vector and expressed the protein in Sf9 cells. Martin *et al*. (1997) did not find functional evidence for h-ezrin activation in Sf9 cells. Moreover, Coscoy *et al*. (2002) have shown that the addition of C-terminal tags does not prevent the dormant configuration of ezrin, so that our C-terminal 6xHis tagged ezrin was expected to be dormant when expressed in Sf9 cells. We purified 6xHis-tagged ezrin from Sf9 cells under nondenaturing conditions. The eluates from the Ni^{2+} column showed a single band of the expected size in Coomassie Blue staining (Figure 7A, left), which, in addition, was recognized by both anti-His tag (our unpublished data) and anti-human ezrin antibodies in immunoblots (Figure 7A, input). These extracts were desalted, concentrated by ultrafiltration, and resuspended in a buffer that enables PKC activity. Then, ezrin was incubated in the presence or absence of recombinant active PKCθ, a kinase known to phosphorylate ezrin T567, and therefore to convert the dormant form into the active form (Simons *et al*., 1998). The success of the phosphorylation was verified by immunoblot with an anti-phospho T567 ezrin mAb (Figure 7A, input). To further verify that ezrin expressed in Sf9 cells is dormant, but can be activated by phosphorylation in T567, we conducted ezrin pull-downs with F-actin covalently attached to Sepharose beads. Identical amounts of phosphorylated (+) or nonphosphorylated (−) ezrin were present in the inputs (Figure 7A), but only PKCθ-phosphorylated ezrin could be pulled down by F-actin (Figure 7A, + pull-down, pellet). The leak of actin from the beads upon SDS elution was used as a control for even load of F-actin-coupled beads. Likewise, Sepharose beads with an irrelevant protein were also used as controls for nonspecific binding (Figure 7A). However, when the supernatants of the pull-down were analyzed, ezrin was found in all the controls and the nonphosphorylated sample, but it was depleted from the F-actin pull-down of the phosphorylated aliquot (Figure 7A, sup.). Although this result did not allow us to conclude that PKCθ-mediated phosphorylation was quantitatively effective, it seems safe to assume that the fraction of ezrin that remained nonphosphorylated in T567 after PKCθ treatment was small and below the threshold of detection in these experiments. Therefore, h-ezrin expressed in Sf9 cells behaves as a dormant form and displays the same biological activity upon T567 phosphorylation as ezrin expressed in mammalian cells.

Having proven that we can express and purify full-length ezrin in the dormant or in the active (after PKCθ phosphorylation) configurations, we proceeded to test direct binding of ezrin to keratins in a blot overlay ("Far-Western") assay. Keratins were highly purified from CACO-2 cells by standard procedures, separated by SDS-PAGE and blotted onto nitrocellulose. The total protein content of each nitrocellulose strip was shown by reversible Ponceau red staining (Figure 7B, lanes P) and showed only three bands. Furthermore, the purity of cytoskeletal preparations obtained by the same protocol has been confirmed elsewhere by two-dimensional electrophoresis and found to contain K8, K18, and K19 (Salas, 1999). The same strips were overlaid with purified active (+) or dormant (−) ezrin, or, as a control, with a V5–6xHis-tagged lacZ expressed in COS cells and purified just like ezrin. Another set of nitrocellulose strips was blotted with various irrelevant proteins including myosin, fumarase (Figure 7B, control proteins), and tropomyosin (our unpublished data), and overlaid with dormant ezrin. After extensive washes the strips were developed as a regular immunoblot (WB) with anti-ezrin, or, when appropriate, with anti-V5 epitope antibody. None of the controls showed binding. Neither did active ezrin bind to keratins nor dormant ezrin bind to the control proteins. In other words, neither ezrin nor keratins seem to nonspecifically bind other proteins. In all four experiments, however, dormant ezrin bound to K18 (Figure 7B), and in one out of four experiments, dormant ezrin also bound to K8 and K19 as well. Although we do not have any explanation for this variability

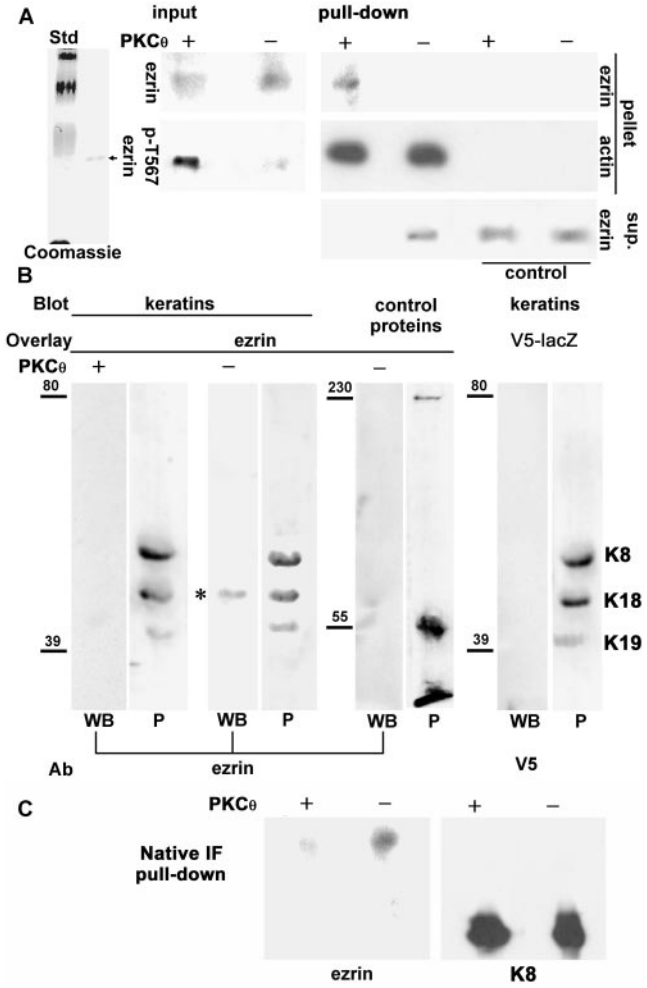

Figure 7. Dormant ezrin binds to keratin and IFs in vitro. (A) The 6xHis-tagged human ezrin was expressed in Sf9 cells and purified under nondenaturing conditions on Ni^{2+} columns. A single-band (arrow) was eluted from the column in 350 mM imidazole and visualized with Coomassie Blue (Std, 201, 127, 86, and 31 kDa). Then, that product was desalted, concentrated, rediluted in PKCθ buffer, and phosphorylated (+) or not (−) with recombinant active PKCθ. Aliquots were analyzed by immunoblot with anti-ezrin and anti-ezrin-pT567 antibodies (input). Purified actin was polymerized, stabilized in 70 nM phalloidin, and covalently attached to CNBr-activated Sepharose. After extensive washes, the beads were incubated in the presence of PKCθ-phosphorylated (+, active) or not (−, dormant) ezrin for pull-down. As a control, beads covalently coupled to an irrelevant protein (nonimmune IgG) were used. The eluates from the pellets were analyzed by immunoblot with anti-ezrin antibody or with an anti-actin antibody to detect the G-actin leaking from the beads under denaturing conditions as a bead load control. The protein in the supernatant after the pull-down (sup.) was precipitated and analyzed by immunoblot with anti-ezrin antibody. (B) Highly purified keratins from CACO-2 cells were separated by SDS-PAGE and blotted onto nitrocellulose. Each strip was transiently stained with Ponceau red (P) to show protein load. The same strips were then incubated with the ezrin preparation tested in A either PKCθ-phosphorylated (+) or not (−). As a control for the ligand, they also were incubated with a V5–6xHis-tagged lacZ expressed in COS cells and purified like ezrin. As a control for the substrate, nitrocellulose strips blotted with fumarase and myosin (control proteins), instead of keratins, were incubated with dormant ezrin. The blots overlaid with ezrin were analyzed by immunoblot with anti-ezrin antibody (WB), or, in the case of the ligand control, with anti-V5 epitope antibody. Numbers to the left of the strips indicate the position of molecular mass markers in kilodaltons. (C) **Figure 7 (cont).** The same input of dormant (−) or active ezrin (+) shown in A was pulled down with a mixture of native highly-purified K8-K18 and K8-K19 IFs coupled to Sepharose beads. The eluate was immunoblotted with anti-ezrin antibody. The right-hand panel shows the same membrane reprobed with anti-K8 antibody as a bead load control.

in the keratin specificity, this result indicates that dormant, but not active, ezrin binds directly to K18, and perhaps to other keratins as well. Finally, because keratins were denatured and in monomeric form for blot overlays, we sought to repeat ezrin binding in vitro, using native, polymerized IFs. To this end, purified IFs were covalently attached to Sepharose beads, and used in standard pull-down experiments, like those shown in Figure 7A. Consistent with the blot overlay results, fourfold more dormant ezrin than active ezrin was pulled down by native IFs (Figure 7C). In fact, the amount of active ezrin recovered from the pull-down was identical to the background binding on beads covered by an irrelevant control protein (our unpublished data). These results support the notion that the subapical Triton-insoluble pool of ezrin described in the previous sections may represent dormant ezrin directly bound to IFs.

DISCUSSION

In differentiated simple epithelial cells, ezrin is localized to the microvilli that lack intermediate filaments. No known domains are present in ezrin or keratins that would suggest the possibility of an interaction. Therefore, the brush-border phenotype of keratin knockdowns (Salas *et al*., 1997) and K8 knockout mice (Ameen *et al*., 2001) was a conundrum for the past few years. The data from stable transfectants here confirmed that intermediate filaments are necessary to organize the brush-border-like F-actin cytoskeleton in CACO-2 cells (Figure 1). In addition, CACO-2-K8a cells also enabled us to determine that the apical ezrin scaffold is stable for at least 2 d upon down-regulation of the IFs (Figure 1E). This might be the case in K8-null mice that still show a relatively normal apical brush border, and a distribution of ezrin (our unpublished data) similar to that described by Berryman *et al*. (1993) in wild-type mice. Crypt enterocytes display apical IFs because of the expression of K7 in these animals (Baribault *et al*., 1994; Ameen *et al*., 2001). Therefore, it is possible that ezrin assembly may use the K7 IFs, just before they become down-regulated at the bottom of the villi, and then ezrin remains stable on its own until the enterocytes desquamate from the tip of the villi ~2 d later. This question will only be fully solved if a K7/K8 double knockout mouse becomes available. On the other hand, because overexpression of ezrin partially rescued the apical F-actin phenotype (Figure 1D), we concluded that the low levels of apically localized ezrin in the K8 knockdown play a role in that phenotype downstream of IFs. Yet, several other possible molecular mechanisms also may contribute to organize the apical F-actin layer. Some of them, for example, could involve the need of IFs as a scaffold for local (apical) signaling processes (Coulombe and Omary, 2002; Paramio and Jorcano, 2002). The data presented here do not rule out that possibility, and, in fact, it is likely that local signaling (e.g., ezrin activation) may cooperate to localize ezrin to the apical domain of simple epithelial cells. Because other mechanisms are still poorly identified, we focused this study on the ezrin–IF interactions. The results of overexpression experiments suggested that keratin IFs participate in the polarization of ezrin. It was paradoxical to find that overexpression

of K8 in HK8 mice hindered the development of the apical brush border (Figure 3), just like the K8 knockdown, with a phenotype resembling that of ezrin knockouts (Saotome *et al*., 2004). The key difference between both phenotypes was the behavior of ezrin. Although ezrin did not seem to assemble anywhere in the CACO-2 K8 knockdown phenotype, it was prominently displayed in the cytoplasm of enterocytes overexpressing K8, coaligning with the supernumerary bundles of IFs, far below the apical membrane.

Using both immunoelectron microscopy and coimmunoprecipitation with IFs, we showed that a modest Triton-insoluble subapical pool of ezrin, attached to IFs is present in differentiated cells (Figure 4). This pool could be increased by an extensive treatment with cytochalasin D, and expressing V5-tagged ezrin in undifferentiated cells. In the second paradigm, V5-ezrin accumulated in the dormant configuration as TX-100-insoluble ezrin around IFs, as opposed to differentiating cells where V5-ezrin readily incorporated into microvilli. Although this result also indicates that other differentiation-dependent processes, presumably ezrin activation, also are necessary to recruit ezrin to the apical domain, this experiment suggests that the attachment to IFs precedes the final assembly. Such a kinetic interpretation was supported by two independent pieces of evidence. First, in pulse-chase experiments, newly synthesized ezrin incorporated in Triton-insoluble complexes with keratins very rapidly (<10 min) and transiently (Figure 6B). It is recognized, however, that coimmunoprecipitation of newly synthesized ezrin with IFs might be mediated by other proteins such as, for example, IF-associated chaperones (Perng *et al*., 1999). The second line of evidence showed that dormant, but not active, ezrin can bind directly to keratins in vitro (Figure 7, B and C). Although this result does not rule out indirect interactions in vivo, it suggests the possibility of direct early binding before ezrin activation. Although we have not measured K_D for this binding, it is clear that the affinity must be at least in the same range of those of antibodies, or these in vitro experiments would not be possible. Together, these data suggest the following model: newly synthesized (dormant) ezrin is rapidly recruited via binding to keratin IFs, which are concentrated (although not exclusively distributed) under the apical domain. This creates a pool of dormant ezrin in the vicinity of the apical membrane that can be locally activated by T567 phosphorylation. On activation, ezrin is released from IFs and incorporated into its final F-actin scaffold. A transient attachment to the membrane upon activation before binding F-actin may explain the temporary decrease in Triton-insoluble ezrin 1 h after translation (Figure 6A), but further investigations are necessary to clarify that issue. This idea of a mostly subapical dormant ezrin reservoir can help us understand why ezrin is not largely assembled in the basolateral domain where F-actin, transmembrane ezrin-binding proteins, and activation mechanisms (e.g., Rho) are available.

It must be pointed out that the mechanism described here may be tissue specific or even restricted to intestinal epithelial cells. Specifically, no effects were found in the brush border of kidney proximal tubules in HK8-4 samples. Likewise, the effects of ezrin depletion may vary in the presence of other ERM proteins. In fact, whether the model proposed here applies to other ERM proteins remains to be studied. Our present studies indicate that IFs play a scaffolding role in tissue-specific functions beyond their traditional "mechanical strength" functions. Understanding how IFs act as organizers of the apical domain in intestinal cells and their relationships with other mechanisms of polarization may provide critical insights into the consequences of mutations in various keratins identified as determinants of bowel, liver, and pancreatic disease in humans (Cavestro *et al*., 2003; Ku *et al*., 2003; Owens *et al*., 2004).

ACKNOWLEDGMENTS

We are grateful to Drs. Richard Rotundo, David Helfman, and Robert Warren for critically reading the manuscript. Yolanda Figueroa provided superb technical help and Susan Decker's aid with EM also was invaluable. TROMA I mAb, developed by Drs. R. Kemler and P. Brulet, was obtained through the Developmental Studies Hybridoma Bank, supported by National Institute on Deafness and Other Communication Disorders, and maintained by the Department of Biological Sciences, University of Iowa. This work was supported by Grant 5RO1DK57805 from National Institute of Diabetes and Digestive and Kidney Diseases (to P.J.I.S.). F.A.W. and A.S.O. were recipients of postdoctoral and predoctoral fellowships, respectively, from American Heart Association, Florida Division.

REFERENCES

Ameen, N. A., Figueroa, Y., and Salas, P.J.I. (2001). Anomalous apical plasma membrane phenotype in CK8-deficient mice indicates a novel role for intermediate filaments in the polarization of simple epithelia. J. Cell Sci. *114*, 563–575.

Bachman, S., Kriz, W., Kuhn, C., and Franke, W. W. (1983). Differentiation of cell types in the mammalian kidney by immunofluorescence microscopy using antibodies to intermediate filament proteins and desmoplakins. Histochemistry *77*, 365–394.

Baribault, H., Penner, J., Iozzo, R. V., and Wilson-Heiner, M. (1994). Colorectal hyperplasia and inflammation in keratin 8-deficient FVB/N mice. Genes Dev. *8*, 2964–2973.

Berryman, M., Franck, Z., and Bretscher, A. (1993). Ezrin is concentrated in the apical microvilli of a wide variety of epithelial cells whereas moesin is found primarily in endothelial cells. J. Cell Sci. *105*, 1025–1043.

Bretscher, A., Reczek, D., and Berryman, M. (1997). Ezrin: a protein requiring conformational activation to link microfilaments to the plasma membrane in the assembly of cell surface structures. J. Cell Sci. *110*, 3011–3018.

Bretscher, A., Chambers, D., Nguyen, R., and Reczek, D. (2000). ERM-Merlin and EBP50 protein families in plasma membrane organization and function. Annu. Rev. Cell Dev. Biol. *16*, 113–143.

Casanova, M. L., Bravo, A., Were, F., Ramirez, A., Jorcano, J. L., and Vidal, M. (1995). Tissue-specific and efficient expression of the human simple epithelial keratin 8 gene in transgenic mice. J. Cell Sci. *108*, 811–820.

Casanova, M. L., Bravo, M., Ramirez, A., Morreale de Escobar, G., Were, F., Merlino, G., Vidal, M., and Jorcano, J. L. (1999). Exocrine pancreatic disorders in transgenic mice expressing human keratin 8. J. Clin. Investig. *103*, 1587–1595.

Cavestro, G. M., Frulloni, L., Nouvenne, A., Neri, T. M., Calore, B., Ferri, B., Bovo, P., Okolicsanyi, L., di Mario, E., and Cavallini, G. (2003). Association of keratin 8 gene mutation with chronic pancreatitis. Dig. Liver Dis. *35*, 416–420.

Coscoy, S., Waharte, F., Gautreau, A., Martin, M., Louvard, D., Mangeat, P., Arpin, M., and Amblard, F. (2002). Molecular analysis of microscopic ezrin dynamics by two-photon FRAP. Proc. Natl. Acad. Sci. USA *99*, 12813–12818.

Coulombe, P. A., and Omary, M. B. (2002). 'Hard' and 'soft' principles defining the structure, function and regulation of keratin intermediate filaments. Curr. Opin. Cell Biol. *14*, 110–122.

Fievet, B. T., Gautreau, A., Roy, C., Del Maestro, L., Mangeat, P., Louvard, D., and Arpin, M. (2004). Phosphoinositide binding and phosphorylation act sequentially in the activation mechanism of ezrin. J. Cell Biol. *164*, 653–659.

Figueroa, Y., Wald, F. A., and Salas, P.J.I. (2002). $p34^{cdc2}$ mediated phosphorylation mobilizes microtubule organizing centers from the apical intermediate filament scaffold in Caco-2 epithelial cells. J. Biol. Chem. *277*, 37848–37854.

Gautreau, A., Louvard, D., and Arpin, M. (2000). Morphogenetic effects of ezrin require a phosphorylation-induced transition from oligomers to monomers at the plasma membrane. J. Cell Biol. *150*, 193–203.

Gouyer, V., Leteurtre, E., Delmotte, P., Steelant, W. F., Krzewinski-Recchi, M. A., Zanetta, J. P., Lesuffleur, T., Trugnan, G., Delannoy, P., and Huet, G. (2001). Differential effect of GalNAc alpha-O-bn on intracellular trafficking in enterocytic HT-29 and Caco-2 cells: correlation with the glycosyltransferase expression pattern. J. Cell Sci. *114*, 1455–1471.

Kotani, H., Takaishi, K., Sasaki, T., and Takai, Y. (1997). Rho regulates association of both the ERM family and vinculin with the plasma membrane in MDCK cells. Oncogene *14*, 1705–1713.

Ku, N. O., Darling, J. M., Krams, S. M., Esquivel, C. O., Keeffe, E. B., Sibley, R. K., Lee, Y. M., Wright, T. L., and Omary, M. B. (2003). Keratin 8 and 18 mutations are risk factors for developing liver disease of multiple etiologies. Proc. Natl. Acad. Sci. USA *100*, 6063–6068.

Kurashima, K., D'Souza, S., Szaszi, K., Ramjeesingh, R., Orlowski, J., and Grinstein, S. (1999). The apical Na(+)/H(+) exchanger isoform NHE3 is regulated by the actin cytoskeleton. J. Biol. Chem. *274*, 29843–298499.

Louvet-Vallée, S. (2000). ERM proteins: from cellular architecture to cell signaling. Biol. Cell *92*, 305–316.

Louvet-Vallée, S. Dard, N., Santa-Maria, A., Aghion, J., and Maro, B. (2001). A major posttranslational modification of ezrin takes place during epithelial differentiation in the early mouse embryo. Dev. Biol. *231*, 190–200.

Martin, M., Roy, C., Montcourrier, P., Sahuquet, A., and Mangeat, P. (1997). Three determinants in ezrin are responsible for cell extension activity. Mol. Biol. Cell *8*, 1543–1557.

Owens, D. W., *et al*. (2004). Human keratin 8 mutations that disturb filament assembly observed in inflammatory bowel disease patients. J. Cell Sci. *117*, 1989–1999.

Perng, M. D., Muchowski, P. J., van Den Ijssel, P., Wu, G. J., Hutcheson, A. M., Clark, J. I., and Quinlan, R. A. (1999). The cardiomyopathy and lens cataract mutation in αB-crystallin alters its protein structure, chaperone activity, and interaction with intermediate filaments in vitro. J. Biol. Chem. *274*, 33235–33243.

Paramio, J. M., and Jorcano, J. L. (2002). Beyond structure: do intermediate filaments modulate cell signalling? Bioessays *24*, 836–844.

Pinto, M., *et al*. (1983). Enterocyte-like differentiation and polarization of the human colon carcinoma cell line Caco-2 in culture. Biol. Cell *47*, 323–330.

Poullet, P. Gautreau, A., Kadare, G., Girault, J. A., Louvard, D., and Arpin, M. (2001). Ezrin interacts with focal adhesion kinase and induces its activation independently of cell-matrix adhesion. J. Biol. Chem. *276*, 37686–37691.

Quaroni, A., Calnek, D., Quaroni, E., and Chandler, J. S. (1993). Keratin expression in rat intestinal crypt and villus cells. Analysis with a panel of monoclonal antibodies. J. Biol. Chem. *266*, 11923–11931.

Regadera, J., Espana, G., Roias, M. A., Recio, J. A., Nistal, M., and Suarez-Quian, C. A. (1997). Morphometric and immunocytochemical study of the fetal, infant and adult human vas deferens. J. Androl. *18*, 623, 636

Rodriguez, M. L., Brignoni, M., and Salas, P.J.I. (1994). A specifically apical sub-membrane intermediate filament cytoskeleton in non-brush-border epithelial cells. J. Cell Sci. *107*, 3145–3151.

Salas, P.J.I. (1999). Insoluble γ-tubulin-containing structures are anchored to the apical network of intermediate filaments in polarized CACO-2 epithelial cells. J. Cell Biol. *146*, 645–657.

Salas, P.J.I., Rodriguez, M. L., Viciana, A., Vega-Salas, D. E., and Hauri, H. P. (1997). The apical sub-membrane cytoskeleton participates in the organization of the apical pole in epithelial cells. J. Cell Biol. *137*, 359–375.

Saotome, I., Curto, M., and McClatchey, A. I. (2004). Ezrin is essential for epithelial organization and villus morphogenesis in the developing intestine. Dev. Cell *6*, 855–864.

Shaw, R. J., Henry, M., Solomon, F., and Jacks, T. (1998). RhoA-dependent phosphorylation and relocalization of ERM proteins into apical membrane/actin protrusions in fibroblasts. Mol. Biol. Cell *9*, 403–419.

Shigeta, M., Sanzen, N., Ozawa, N., Gu, J., Hasegawa, H., and Sekiguchi, K. (2003). CD151 regulates epithelial cell-cell adhesion through PKC- and CDC42-dependent actin cytoskeletal organization. J. Cell Biol. *163*, 165–176.

Simons, P. C., Pietromonaco, S. F., Reczek, D., Bretscher, A., and Elias, L. (1998). C-terminal threonine phosphorylation activates ERM proteins to link the cell's cortical lipid bilayer to the cytoskeleton. Biochem. Biophys. Res. Commun. *253*, 561–565.

Steinert, P., Zackroff, R., Aynardi-Whitman, M., and Goldman, R. D. (1982). Isolation and characterization of intermediate filaments. Methods Cell Biol. *24*, 399–419.

Takaishi, K., Sasaki, T., Kotani, H., Nishioka, H., and Takai, Y. (1997). Regulation of cell-cell adhesion by rac and rho small G proteins in MDCK cells. J. Cell Biol. *139*, 1047–1059.

Toivola, D. M., Krishnan, S., Binder, H. J., Singh, S. K., and Omary, M. B. (2004). Keratins modulate colonocyte electrolyte transport via protein mistargeting. J. Cell Biol. *164*, 911–921.

Tran, D., Stelly, N., Tordjmann, T., Durroux, T., Dufour, M. N., Forchioni, A., Seyer, R., Claret, M., and Guillon, G. (1999). Distribution of signaling molecules involved in vasopressin-induced Ca2+ mobilization in rat hepatocyte multiplets. J. Histochem. Cytochem. *47*, 601–616.

Van Aelst, L., and Symons, M. (2002). Role of Rho family GTPases in epithelial morphogenesis. Genes Dev. *16*, 1032–1054.

Van Furden, D., Johnson, K., Segbert, C., and Bossinger, O. (2004). The C. elegans ezrin-radixin-moesin protein ERM-1 is necessary for apical junction remodelling and tubulogenesis in the intestine. Dev. Biol. *272*, 262–276.

Voltz, J. W., Weinman, E. J., and Shenolikar, S. (2001). Expanding the role of NHERF, a PDZ-domain containing protein adapter, to growth regulation. Oncogene *20*, 6309–6314.

Walsh, S. V., Hopkins, A. M., Chen, J., Narumiya, S., Parkos, C. A., and Nusrat, A. (2001). Rho kinase regulates tight junction function and is necessary for tight junction assembly in polarized intestinal epithelia. Gastroenterology *121*, 566–579.

Weibel, E. R. (1979). Stereological Methods, London: Academic Press.

Weinman, E. J., Steplock, D., Donowitz, M., and Shenolikar, S. (2000). NHERF associations with sodium-hydrogen exchanger isoform 3 (NHE3) and ezrin are essential for cAMP-mediated phosphorylation and inhibition of NHE3. Biochemistry *39*, 6123–6129.

Weinman, E. J., Steplock, D., Wade, J. B., and Shenolikar, S. (2001). Ezrin binding domain-deficient NHERF attenuates cAMP-mediated inhibition of Na(+)/H(+) exchange in OK cells. Am. J. Physiol. *281*, F374–F380.

Yonemura, S., Matsui, T., Tsukita, S., and Tsukita, S. (2002). Rho-dependent and -independent activation mechanisms of ezrin/radixin/moesin proteins: an essential role for polyphosphoinositides in vivo. J. Cell Sci. *115*, 2569–2580.